Visualizing Correlation Regions: The Case of the Ammonia Crystal

David Ramírez-Palma,[a] Bruno Landeros-Rivera,[b] Alessandro Genoni,[c] Fernando Cortés-Guzmán,[a] and Julia Contreras-García*[b]

We resort to X-ray constrained wavefunctions in order to separately analyze crystal field and correlation effects in ammonia. With this aim in mind, we compare the electron density and the amount of electron localization in different molecular regions derived from three different calculations: the isolated molecule, the solid-state and the X-ray constrained wavefunctions. While the crystal field effects lead to a contraction (localization) of electron pairs, the introduction of correlation as a correction from the experimental density leads to a compensating effect that diffuses back again the electron pairs. We have also compared the effect on the most widely used methods in solid state, HF and DFT, showing that (as in molecules) correlation has well differenciated effects, with DFT overdelocalizing. It is now well known that approximate functionals have errors in the density reconstruction and in the energy estimation. Resorting to experimental densities thus allows expanding the separation of the errors in the functional and the density in solid state, where correlated wavefunctions are not easily available.

1. Introduction

Correlation energy is defined as the difference between the exact and Hartree-Fock energies. Even though it constitutes a minimal part of the energy of the system, typically around 1%, it is responsible for some of the most important chemical phenomena. As an example, correlation is fundamental to understand dispersive interactions, which dominate the kinetics of reactions through the stabilization of transition states.[1] Within wavefunction approaches, correlation is usually estimated resorting to highly accurate calculations, being CCSD(T) the gold-standard, but these post-HF calculations are extremely costly and hence their application is not feasible for big systems. This is especially the case of solid-state calculations, where correlation estimates have only recently been implemented in some widespread codes.[2] In general, solid-state codes are dominated by Density Functional Theory, where the lack of systematic improvements makes it very difficult to estimate the effects of correlation. This is especially worrisome if we consider that correlation dominated behaviors, such as superconductivity or topological insulators, have become hot topics within the solid-state community. As an example, topological insulators have given rise to more than 70,000 citations in 2020 and 470,000 citations over the years (Web of Science, 2021). Hence, estimating the relevance of correlation in solid-state has become an unsolved issue, where two opposite aspects compete: big systems require the use of DFT, but DFT does not always provide a good estimate of correlation.

An alternative way has recently been developed, which opens the door for the estimation of correlation in solid-state. Jayatilaka and Grimwood[3] proposed to couple single-determinant wavefunctions (HF and DFT) with experimental X-ray diffraction data. More recently some multi-determinant wave function approaches have been also recently proposed.[4–7] Within DFT, two errors are usually coupled: those coming from using incorrect densities, and those due to the lack of the exact functional. The work by Burke *et al.*,[8–10] where DFT energetics was corrected thanks to the use of HF densities, was the first indicator that electron densities must be properly taken into account. The final proofs in this direction came in 2017,[11,12] when some functionals were shown to lead to important errors in the electron density, in spite of improvement in the energies. The alternative correction method consists in resorting to the experimental densities. Once these densities have been corrected for thermal effects, they provide the perfect basis for i) separating density-functional effects and ii) estimating the errors coming from the lack of correlated densities. It is important to recall that both DFT and HF are related to errors in the electron density that can be collected under the umbrella of "delocalization error". Density functionals tend to overdelocalize and artificially spread electrons in the molecule.[13,14] Instead, HF tends to localize the charges on the core of the atoms.[15] Hence, the inclusion of correlation with the Jayatilaka

[a] Dr. D. Ramírez-Palma, Dr. F. Cortés-Guzmán
Universidad Nacional Autónoma de México,
Instituto de Química, Ciudad Universitaria
Ciudad de México, 04510
[b] Dr. B. Landeros-Rivera, Dr. J. Contreras-García
CNRS, Laboratoire de Chimie Théorique,
LCT, Sorbonne Université,
Paris, France
E-mail: contrera@lct.jussieu.fr
[c] Dr. A. Genoni
Université de Lorraine & CNRS,
Laboratoire de Physique et Chimie Théoriques (LPCT),
UMR CNRS 7019, F-57078 Metz, France

Supporting information for this article is available on the WWW under https://doi.org/10.1002/cmtd.202100045

and Grimwood approach should directly reflect the effects of delocalization error, enabling to also narrow down the errors in the functional.

The X-ray constrained wavefunction (XCW) strategy proposed by Jayatilaka and Grimwood is formally a single molecule-like technique that consists in finding the wavefunction that not only minimizes the energy of the system under examination, but that also reproduces collected experimental X-ray structure factors amplitudes within the limit given by the experimental uncertainties. In other words, the method aims at minimizing the following functional:

$$L[\Psi] = E[\Psi] + \lambda \chi^2, \tag{1}$$

where $E[\Psi]$ is the electronic energy of the system, χ^2 is the statistical agreement between experimental and calculated structure factor amplitudes (see below for more details), λ is an external multiplier that is manually adjusted during the calculations and that gives the strength of the experimental constraints. For the sake of precision, it is important to note that the method does not introduce any constraint on the single values of the structure factor amplitudes. In fact, the method should be better renamed as X-ray restrained wavefunction (XRW) technique, as it was actually already proposed by Ernst *et al.* in a previous work that mainly aimed at studying the capability of the Jayatilaka approach in capturing the crystal field effects on the electron density.[16]

In particular, the χ^2 statistical agreement between the computed and experimental structure factor amplitudes ($F^c(\mathbf{h})$ and $F^{exp}(\mathbf{h})$, respectively) is given by this expression:

$$\chi^2 = \frac{1}{N_r - N_p} \sum_{\mathbf{h}} \frac{[\eta F^c(\mathbf{h}) - F^{exp}(\mathbf{h})]^2}{\sigma(\mathbf{h})^2}, \tag{2}$$

with N_r as the total number of unique reflections, N_p as the number of adjustable parameters used (usually only the external parameter λ), $\mathbf{h}$ as the triad of Miller indices which characterizes the reflection, $\sigma(\mathbf{h})$ as the experimental uncertainty associated with the experimental structure factor amplitude $F^{exp}(\mathbf{h})$, and η as an overall $\mathbf{h}$-independent scale factor that puts $F^c(\mathbf{h})$ on the same scale of $F^{exp}(\mathbf{h})$. It is worth noting that, by definition, χ^2 is the probability distribution towards which a distribution of random squared differences tends. In this case, χ^2 is normalized by the number of degrees of freedom ($N_r - N_p$). Therefore, for an adequate model and proper weights, the XCW calculations should stop when $\chi^2 = 1$,[17] which is the expected value for the normalized sum of weighted squared differences in equation (2) (i.e, the sum of the squared differences of the calculated and experimental structure factor amplitudes divided by the corresponding squared experimental uncertainties), if they are assumed as uncorrelated Gaussian random numbers with a mean value of zero.

To cite a few examples of applications, the *XCW* approach has been used to carry out the topological analysis of crystal fragments,[18] to investigate the effect of the crystalline environment[19] and to analyze non-centrosymmetric crystals.[20] The respective wavefunctions have also been the aim of in-depth theoretical chemistry analyses, as the availability of orbitals from experimentally constrained optimizations enabled the reconstruction of Electron Localization Indicator (ELI)[21] and Extremely Localized Molecular Orbitals[22,23] from X-ray diffraction data. Indeed, having access to the orbitals, enables to analyze electron localization. Note that the localization concepts throughout the text refer to real space localization, understanding by such the localization of electron pairs as revealed in non-metallic cases by localized orbitals and localization indexes such as ELF or LOL. These viewpoints converge in the case of perfectly localized orbitals.[24] In order to avoid problems of selection of orbitals, here we will mainly focus on the Electron Localization Function (ELF). ELF has been shown to provide a measure of electron pairing by means of kinetic energy densities.[25] Starting from a monodeterminantal kinetic energy density, $t(\mathbf{r})$, and taking away the bosonic contribution (second term in the righthandside of equation 3), we have the so-called Pauli kinetic energy density, t_P:

$$t_P(\mathbf{r}) = t(\mathbf{r}) - \frac{1}{8}\frac{|\nabla\rho|^2}{\rho} \tag{3}$$

Note that the bosonic contribution is an imaginary reference where all electrons are placed in the same orbital to yield the fermionic calculated electron density. This reference allows to get insight into the increased local speed of electrons due to their fermionic nature. This quantity is then divided by the Thomas-Fermi kinetic energy density, t_{TF}, and remapped so that it runs from 0 to 1:

$$ELF = \frac{1}{1 + (\frac{t_P}{t_{TF}})^2} \tag{4}$$

In this way, ELF is close to 1 when electrons are localized (e.g. atomic shells, bonds and lone pairs) and close to 0 in between highly localized regions.

The aim of this work is to expand the analysis performed by Jayatilaka and collaborators in a series of publications related to localization and the crystal environment of ammonia.[19,20,26] In those previous reports, the analysis focused on the effects of the crystal environment on the electron localization. They used electron localization function and the Fermi hole mobility function to distinguish the electron localization information derived from X-ray constrained wavefunctions for crystals of ammonia, urea and alloxan. They found that the electron density flows from the lone-pair region to the opposite side of the nitrogen atom (between the hydrogen atoms) for ammonia.[26] For the sake of completeness, in this context it is also worth mentioning two separate studies that aimed at evaluating the capability of the XCW approach in capturing electron correlation and crystal field effects on the electron density, although, in those investigations, only theoretically-generated structure factors were used.[16,27]

In this work, we would like to focus our attention on the effects of electron correlation on the electron density, introduced by the use of experimental X-ray data as compared to correlation-lacking calculations. In addition, we will also

compare different computational approaches, as a way to elucidate their effects on the electron density as we go from the isolated molecule to the crystal.

2. Results and Discussion

We will first analyze the changes in energy and electron density as λ increases. Results depend on the choice of the (χ^2, λ) pair. Hence, in the following we will focus on each part of this pair. First we will focus on a given χ^2, i.e. a similar agreement with experimental data. Secondly, we will briefly focus on results for a given λ, i.e. on the influence of a given weight from the experimental data constraints.

2.1. Electron Density and Energy

Figure 1 shows the agreement between experimental data and the XCW and the changes in energy for HF and DFT calculations, as the λ value increases ($\Delta E = E_\lambda - E_{\lambda=0}$). It is easily noted that as the agreement between theory and experiment increases (i.e. χ^2 decreases), the energy of the system increases as expected from the variational principle. Indeed, for HF(DFT) the minimal energy is obtained for the converged SCF at $\lambda = 0$, so including a constraint (even if it goes towards more "correct" densities) will increase the calculated energy.

However, different trends are observed for HF and DFT. At the beginning ($\lambda = 0$), DFT calculations have better agreement with experiment than HF: $\chi^2 = 9.34$ and 10.89, respectively. However, from $\lambda = 0.002$ both HF and DFT lead to similar results with negligible χ^2 differences (see $\Delta\chi^2$ vs λ in Figure S1).

Nevertheless, from this point on, the changes in $\Delta\Delta E = \Delta E_{HF} - \Delta E_{DFT}$ increase significantly, with DFT providing lower energies (see $\Delta\Delta E$ vs λ in Figure S1).

The point where $\chi^2 \approx 1.0$ is usually taken as the reference (green line in Figure 1). In spite of the fact that this occurs at nearly the same λ value for both methods ($\Delta\lambda_{HF-DFT} = -0.0011$), the ΔE_{HF} is noticeably larger for HF. This is in agreement with recent DFT developments, in which HF densities are found to be closer to the real ones, but the lack of opposite spin correlation leads to better energy estimates from DFT.[8] Finally, for large λ values, the changes in energy are more important than the changes in χ^2, thus becoming an unrealistic physical situation. The final χ^2 obtained with $\lambda = 0.03$ was 0.57 for HF and 0.58 for DFT.

The effects of λ on the electron density are subtle at this level, but can be followed thanks to the topology of the atomic graph of nitrogen. The atomic graph condenses the information of the Laplacian of the electron density, $\nabla^2\rho(\mathbf{r})$, in a set of critical points (*CPs*) and atomic graph paths. The set of critical points needs to satisfy Euler's formula for a polyhedron $V - E + F = 2$, where V corresponds to the vertices (or local charge concentrations regions, *CC*), E are the edges and F are the faces (or local charge depletion regions, *CD*). Each critical point is classified with the index $(\omega, \pm\sigma)$ where ω and $\pm\sigma$ are its range and signature of the eigenvalues in the Hessian matrix of $\nabla^2\rho(\mathbf{r})$. The vertices correspond to $(3, +3)$ *CPs*, the edges are formed between a pair of flux lines originated from $(3, +1)$ *CPs*, and every face in the polyhedron has a $(3, -1)$ *CP* in the center. Figure 2 shows the atomic graph of the nitrogen atom in the ammonia molecule calculated at the point where $\chi^2 \approx 1.0$ with the HF method (similar results are found for DFT, see Figures S2 and S3 in S.I.).

In order to follow the main localization regions, we focus on the *CPs* related to the lone pair of the nitrogen atom and the N–H bond (see Figure 2). Figure 3 shows the behavior of these *CPs* as λ increases. It can be seen that λ has an opposite effect on the lone pair and the N–H bond. Introducing the constrain to fit experimental data leads to the the delocalization of the nitrogen lone pair: it moves away from the nitrogen core and decreases its charge concentration (less negative Laplacian). Instead, the N–H bond localizes: its charge increases (more negative Laplacian) and it comes closer to the nitrogen core. These are the expected results for HF: the most delocalized unit, the lone pair, was overlocalized with HF, so it delocalizes

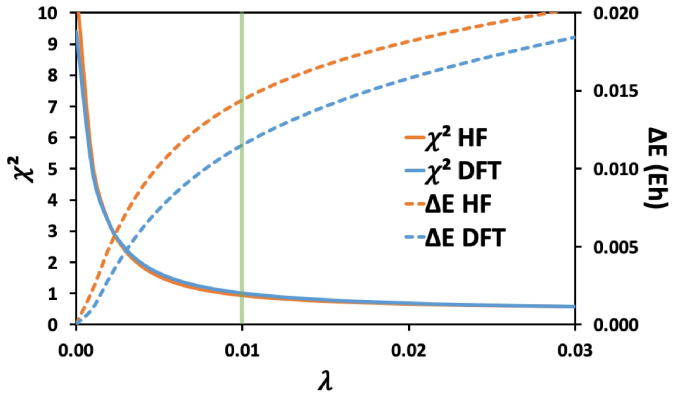

Figure 1. Variation of agreement statistic, χ^2, and changes in total energy, ΔE, with λ values for HF and DFT (B3LYP) calculations in NH_3.

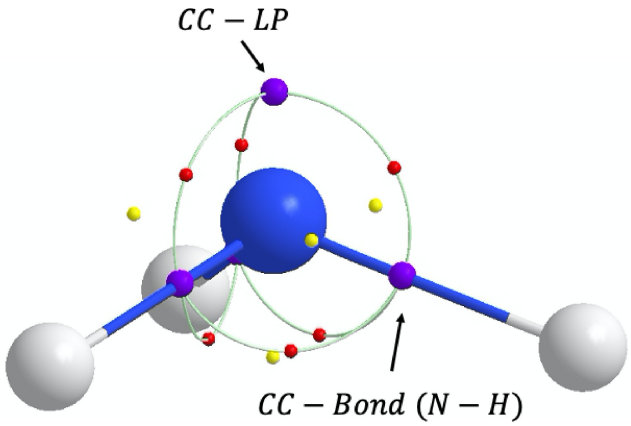

Figure 2. Atomic graph of nitrogen atom in ammonia molecule resulting from an XCW calculation at HF level with $\chi^2 \approx 1.0$. $(3, +3)$ *CPs*, represented with purple color, are *CC* critical points, (3,–1) *CPs*, yellow points, correspond to *CD* critical points and red points are $(3, +1)$ *CPs*. The critical points of charge concentration in the region of the lone pair (LP) and bond between N–H atoms are indicated.

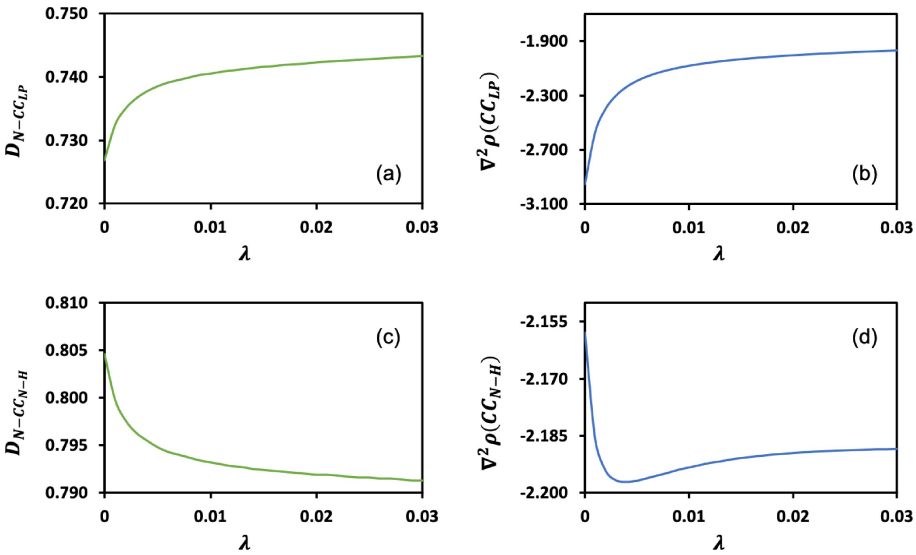

Figure 3. Changes in the distance between nitrogen atom and charge concentration critical point, D_{N-CC}, and changes in $\nabla^2\rho(\mathbf{CC})$ of charge concentration critical points in the lone pair (LP), (a) and (b), or in the direction of the N–H bond (N–H), (c) and (d), as λ increases for an XCW calculation at HF level. All quantities in atomic units.

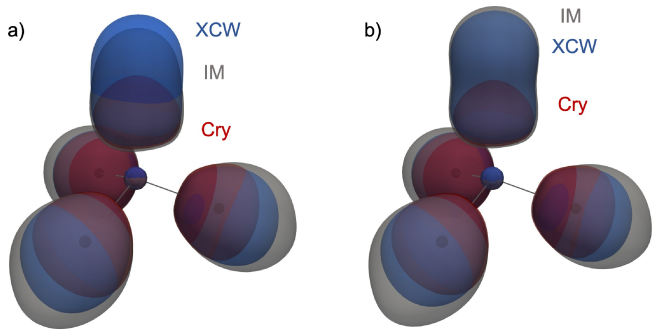

Figure 4. 3D plots of the *ELF* (isovalue 0.9) for a) HF and b) DFT ammonia molecule calculations in *IM* (grey), *XCW* (blue), and *Cry* (red).

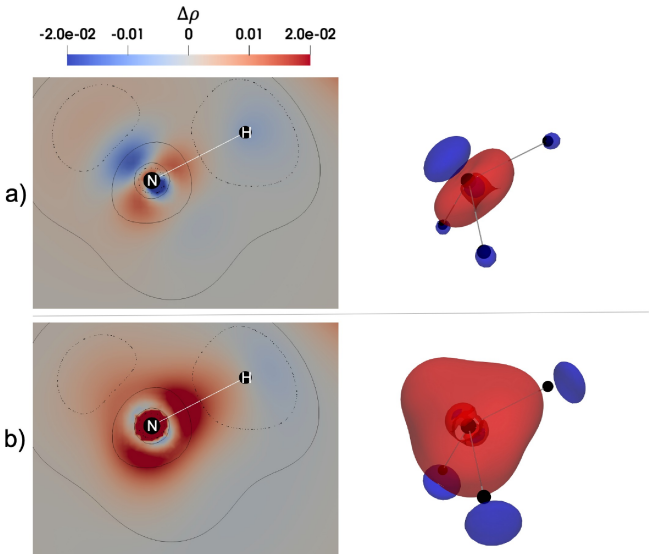

Figure 5. Plots in 2D and 3D of ρ difference between *Cry* and *IM* for a) HF and b) DFT ammonia molecule calculations ($\Delta\rho = \rho_{Cry} - \rho_{IM}$). Contours with the isovalues 0.5 (continuous line) and 0.9 (dotted line) of *ELF* in Cry. Isosurfaces with negative values (−0.005 a.u. for HF and −0.003 a.u. for DFT) in blue and positive values (0.005 a.u.) in red.

as λ increases. On the contrary, for bonds we observe a localization when correlation effects are introduced.

2.2. Crystal Field and Correlation Effects

This section focuses on results for $\chi^2 \approx 1$ with experimentally constrained HF and DFT calculations ($\lambda = 0.0089$, $\chi^2 = 0.9969$ for HF and $\lambda = 0.0103$, $\chi^2 = 0.9980$ for DFT) and the def2-TZVP basis set. It is interesting to analyze the effects of crystal field and electron correlation described by the XCW wavefunction as the result of two separate steps: at a first step passing from the molecular calculation (*IM*) to the solid-state calculation (*Cry*) with the same method (i.e. $\lambda = 0$) shows the crystal field effects. At a second stage, comparing the solid-state calculation with the X-ray constrained wavefunction (*XCW*, $\lambda \neq 0$) shows the effect of correlation overestimated by DFT (HF). Figure 4 shows the effects on the 3D localization of these two progressive stages thanks to the *ELF* isosurfaces at *ELF* = 0.9. In order to compare the different effects depending on the method, both HF (Figure 4a) and DFT (Figure 4b) are shown side by side for the same basis set (def2-TZVP).

If we look at the general image of ELF, we see that a similar chemical interpretation appears, which is in agreement with Lewis' structure: 3 N–H basins and the nitrogen lone pair. However, when plotted together, we can see slight differences introduced by the environment and the method. Both within HF and DFT, the crystal field effects (*IM* → *Cry*) lead to a contraction of the electron pair regions due to Pauli repulsion. The crystal field effects are thus qualitatively similar for all basins and methods. However, it is quantitatively different

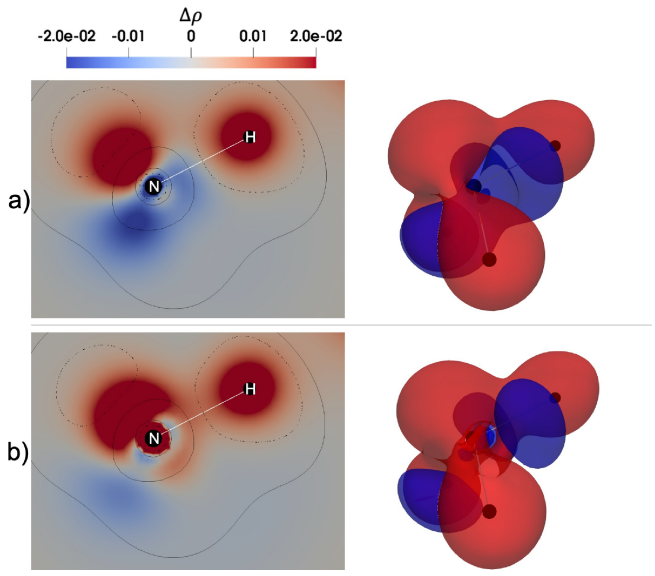

Figure 6. Plots in 2D and 3D of ρ difference between *Cry* and *XCW* for a) HF and b) DFT ammonia molecule calculations ($\Delta\rho = \rho_{Cry} - \rho_{XCW}$). Contours with the isovalues 0.5 (continuous line) and 0.9 (dotted line) of *ELF* in Cry. Isosurfaces with negative values (−0.005 a.u.) in blue and positive values (0.005 a.u.) in red.

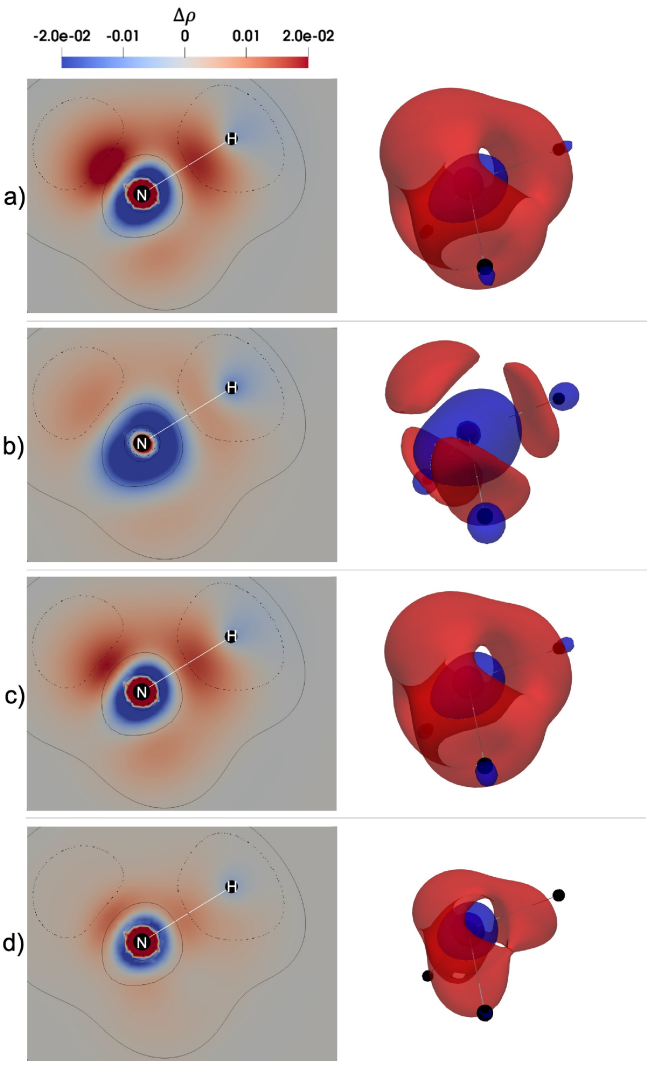

Figure 7. Plots of the difference in electron density between HF and DFT methods for a) *IM*, b) *Cry*, c) $XCW_{\lambda=0.001}$ and d) $XCW_{\lambda=0.030}$ for ammonia molecule ($\Delta\rho = \rho(\mathbf{r})_{HF} - \rho(\mathbf{r})_{DFT}$). Isosurfaces with negative values (−0.005 a.u.) in blue and positive values (0.005 a.u.) in red. Contours in plots with the isovalues 0.5 (continuous black line) and 0.9 (dotted black line) of the *ELF* in *Cry*.

between hydrogen and lone pair basins, being the volume change especially noticeable in the most delocalized unit, i.e. the lone pair. The lone pair volume contained within the 0.9 isovalue is bigger for the isolated molecule in DFT calculation and for the XCW in HF calculation. However, as the molecule is introduced in the crystal, the volume becomes very compact. This is directly related to the high compressibility of the lone pair basin.[28] Overall, this behavior is in agreement with the observations by previous authors who analyzed crystal field effects from theoretical calculations.[26]

It is interesting to add an extra step thanks to constrained wavefunctions which enables us to analyze the effect of correlation on this theoretical ammonia crystal. The effect of introducing the correlation on the calculation leads to more differential behaviors. Electron correlation increases the "repulsion" between electrons, leading to the breathing of the localization regions, which regain greater volumes with respect to the contracted *Cry* calculation. This is similar to the lowering of the bond order, reflected in the decrease of the value of the electron density at the bond critical points, as it was already observed in molecules.[27,29–32] However, in this case, changes are very different depending on the nature of the basin. While changes in the N–H bonds are small, changes in the lone pair are much bigger. The volume of the lone pair basins goes back to a volume similar to the one in the isolated molecule so that crystal field and correlation effects nearly counteract each other. These observations are extremely relevant from the point of view of solid-state simulations. Although extended solids will be rather well reproduced by HF or DFT methods, structures with voids will be more prone to error due to an incorrect description of the lone pairs. This can be related to the well-known failure of functionals to describe low dimensional structures (chaltrates, layers, rods), which is usually approached from a dispersion perspective. However, we see here that electron density errors also underlie.

Slight differences are also observed when we compare HF and DFT. Since ELF differences are not meaningful due to the renormalization (equation 4), we will dwell on these differences in terms of electron density difference maps, $\Delta\rho$, from *IM* to *Cry* and from *Cry* to *XCW* in Figures 5 and 6, respectively.

In Figure 5 where $\rho_{Cry} - \rho_{IM}$ is plotted, negative values (blue color) correspond to regions where the electron density is larger in the *IM* than the *Cry* whereas positive values (red color) correspond to a larger concentration of the electron density in the crystal. We can see a flux of the electron density from externally localized areas in the *IM* (H atoms and lone pair) to the internal region of the molecule in the *Cry*. In other words, the effect of the crystal field is to compact the delocalized

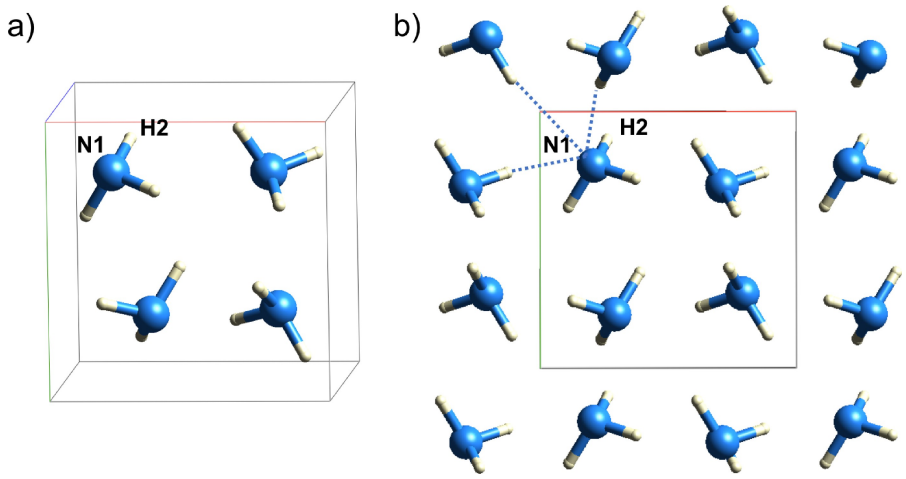

Figure 8. a) Unit cell of ammonia. b) Hydrogen bonding in crystalline ammonia.

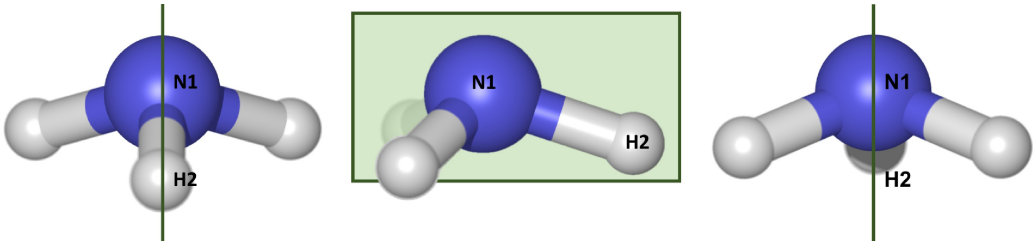

Figure 9. Schematic representation of the plane used to show the results.

regions. This is in agreement with the fact that hydrogen bonds are formed, which takes away charge from the lone pair and injects it into the N–H bonds, while relaxing the Pauli repulsion that appears in between electron pairs from different molecules.

For this step, differences between HF and DFT remain very small: in both methods, the inclusion of the molecule in the crystal leads to similar electron density deformations, with slightly larger changes being observed in DFT. This is in agreement with the localization error.[33] Since DFT tends to overdelocalize, the localization effect of the crystal field is larger in DFT.

Correlation is generally expected to decrease the population of electron pairs, and most specifically, it is known to decrease the HF bond order. This can be observed by comparing the electron density distribution associated with the constrained wavefunction and the solid-state calculation. Figure 6 is the difference of ρ in *Cry* and the *XCW* calculations. Negative values (blue color) correspond to regions with more electron density in the *XCW* and positive regions (red color) indicate bigger values of the electron density in the *Cry*. As we observed in the ELF patterns, overall correlation counteracts the effect of the crystal field.

In Figure 6 we can observe that the electron density flows from the localized regions in the molecule (red) to intermolecular regions (blue), due to greater delocalization in the correlated solution. In the case of HF we can also observe a flow towards the N–H interatomic line (these effects are more visible in the 3D isosurfaces). For DFT, in addition to the different shape already observed for the lone pair, we can see important differences around the nitrogen core at two different distances, corresponding to the shells, which were not enough correlated, and hence they lose density. Both for HF and DFT, the N–H bond electron density needs to be corrected, though in opposite directions: while correlation increases the electron density from the HF result, it decreases it from the DFT one.

2.3. Effects of the Method (λ Fixed)

In order to further dwell on the effects of the monodeterminantal method when introducing experimental constraints, we will now look at the results obtained by fixing the parameter λ in XCW_{HF} and XCW_{DFT} calculations. Figure 7 shows the electron density differences between the HF and DFT calculations in the *IM*, *Cry*, and *XCW* ($\lambda = 0.001$ and $\lambda = 0.03$) cases. Negative values are represented in blue color and correspond to a bigger electron density with the DFT calculation whereas positive values in red color imply more electron density when the HF approach is used. Differences in the *IM* and *Cry* cases follow the general pattern: HF locates more density on the core and bonds regions, whereas DFT tends to localize electron density close to the valence shell of the atoms.

Let us now focus on the effect of introducing electron correlation by the XCW procedure. In this case, the main differences appear around the nitrogen atom, and not the hydrogen ones. We see again the spherical deformation appearing as a shell around the N atom, confirming that this is an effect of the correlation independent of the value of the λ parameter.

As correlation is progressively introduced by increasing λ, smaller HF vs DFT differences appear, which signals that both levels of theory are converging to the same result. In the case of $\lambda = 0.001$, the value of χ^2 is greater for the HF calculation than the DFT (5.129 and 4.864 respectively). This contrast results in a greater difference in the electron density distribution between the two methods. Specifically, a greater localization in the HF method in the area of N–H bond and in the lone pair of nitrogen atom (red regions in Figure 7c). On the other hand, electron localization in DFT is centered around nuclear positions. When we focus on a larger experiment-theory admixture ($\lambda = 0.030$) the values of χ^2 are: $\chi^2_{HF} = 0.565$ and $\chi^2_{DFT} = 0.582$. This demonstrates that correlation included by means of the experimental constraints should lead to similar results in HF and DFT.

3. Conclusions

In this paper, we showed a description of the distribution of the electron density in the ammonia molecule and crystal. Depending on the environment in which the molecule is (isolated molecule or solid-state), the effect of the correlation and the Pauli repulsion will be more important. In solid-state, the crystal field is responsible for a localization effect that moves the electron density from delocalization areas (lone pair and inter-molecular region) to localization areas (bond N–H). On the other hand, the *XCW* calculation is a buffer between the *IM* and the *Cry* governed by a delocalization effect from the bonds to inter-molecular regions. However, using the same amount of constraint for XCW_{HF} and XCW_{DFT} calculations, it is possible to observe a greater localization of electron density in different regions of the molecule. In HF calculations the electron density tends to be higher in the bond regions and the lone pair than for the DFT calculations. In DFT calculations the electron density is higher in the hydrogen atoms and between the bonds than for HF calculations. This allows expanding the analysis of errors in the density induced by approximate functionals (whose relevance has been highlighted in the last years) to solid state, where correlated wavefunctions are not easily available. Instead, experimental densities are taken as the reference, to highlight the errors in the density introduced by the different approaches commonly used in the literature.

Experimental Section

XCW Data

NH_3 data are taken for a cubic cell,[34] Figure 8a, with space group $P2_13$. The rest of the experimental details are reported in Table 1. There are three weak hydrogen bonds formed between the lone pair of the nitrogen atom and 3 hydrogen atoms of 3 different ammonia molecules, Figure 8b.

The *XCWs* were obtained using the program Tonto[35] at HF and DFT (B3LYP)[36,37] levels of theory, and def2-TZVP basis set.[38] The constraining parameter λ was initially set to zero and increased in steps of 0.0005, up to 0.03. The choice of the data was guided by the fact that it lacks high-order reflections, a condition that was shown to be necessary[27] in order to extract a large amount of correlation from XCW calculations.

Computational Details

XCWs were compared with those resulting from solid-state and isolated molecule gas-phase calculations performed with the CRYSTAL[39] and Tonto[35] programs respectively at the same level of theory (HF or B3LYP, def2-TZVP). The difference between gas and solid phases was examined by comparing the distribution or behavior of the electron density, $\rho(\mathbf{r})$, and the electron localization function, *ELF*.[40]

For ammonia, we expect 5 regions of localization (electron pairs): the nitrogen core, the three N–H bonds and the nitrogen lone pair. Since we are interested in analyzing the effects of correlation on the electronic distribution and its localization, we will focus on the regions of expected high *ELF* value in NH_3. In this sense, the plane used to show the results in 2D plots contains the bond N–H and the lone pair of the nitrogen atom, marked in green in Figure 9.

Cube files of the studied scalar fields were obtained for each calculation. In the case of differences between methods, we used the operations of cube files in Multiwfn program[41] and the visualization was performed with Paraview software.[42,43] For a better appreciation of the isosurfaces in 3D it was necessary to modify the origin of the cube files. To match the coordinates of the volumetric data, the Transform tool in Paraview was used. For the topological analysis of the Laplacian of electron density, the wfn file was obtained directly from Tonto using the molecular orbitals for each λ value. The local properties and atomic graphs were computed and visualized with the AIMALL package.[44]

Table 1. Experimental details for the Ammonia crystal structure. Chemical formula = NH_3; space group = $P2_13$, $Z = 4$.

Crystal data		Data collection	
a (Å)	5.1305	Diffractometer (Wavelength)	Nicolet R3m/V four-circle (0.71069 Å)
b (Å)	5.1305	Refinement model	multipole
c (Å)	5.1305	No. of collective reflections	334
α (°)	90	R(%)/Rw(%)	1.19/0.95
β (°)	90	GOF	0.91
γ (°)	90	No. of unique reflections	88
V (Å^3)	135.05	A criterion for obs. Reflections	$F(h) > 3\sigma(h)$

Acknowledgements

Authors acknowledge PAPIIT/DGAPA/UNAM/ECOS (Grants IN202717, IN212520, ECOS C17E09) for financial support, and DGTIC-UNAM (LANCAD-UNAM-DGTIC-194) for computer time. D R–P thanks CONACyT-México for scholarship 293294 and Campus France MX18-01626. B L–R. thanks CONACyT (CVU 366057) for the posdoctoral scholarship.

Conflict of Interest

The authors declare no conflict of interest.

Keywords: crystals · experimentally constrained wavefunctions · isolated molecules · theoretical methods

[1] J. L. Arbour, H. S. Rzepa, J. Contreras-García, L. A. Adrio, E. M. Barreiro, K. K. Hii, *Chem. Eur. J.* **2012**, *18*, 11317–11324.
[2] C. Pisani, L. Maschio, S. Casassa, M. Halo, M. Schütz, D. Usvyat, *J. Comput. Chem.* **2008**, *29*, 2113–2124.
[3] D. Jayatilaka, D. J. Grimwood, *Acta Crystallogr. Sect. A* **2001**, *57*, 76–86.
[4] A. Genoni, *Acta Crystallogr. Sect. A* **2017**, *73*, 312–316.
[5] N. Casati, A. Genoni, B. Meyer, A. Krawczuk, P. Macchi, *Acta Crystallogr. Sect. B* **2017**, *73*, 584–597.
[6] A. Genoni, D. Franchini, S. Pieraccini, M. Sironi, *Chem. Eur. J.* **2018**, *24*, 15507–15511.
[7] A. Genoni, G. Macetti, D. Franchini, S. Pieraccini, M. Sironi, *Acta Crystallogr. Sect. A* **2019**, *75*, 778–797.
[8] M.-C. Kim, E. Sim, K. Burke, *Phys. Rev. Lett.* **2013**, *111*, 073003.
[9] M.-C. Kim, E. Sim, K. Burke, *J. Chem. Phys.* **2014**, *140*, 18A528.
[10] M.-C. Kim, H. Park, S. Son, E. Sim, K. Burke, *J. Phys. Chem. Lett.* **2015**, *6*, 3802–3807.
[11] M. G. Medvedev, I. S. Bushmarinov, J. Sun, J. P. Perdew, K. A. Lyssenko, *Science* **2017**, *355*, 49–52.
[12] K. R. Brorsen, Y. Yang, M. V. Pak, S. Hammes-Schiffer, *J. Phys. Chem. Lett.* **2017**, *8*, 2076–2081.
[13] P. Mori-Sánchez, A. J. Cohen, W. Yang, *Phys. Rev. Lett.* **2008**, *100*, 146401.
[14] J. P. Perdew, R. G. Parr, M. Levy, J. L. Balduz Jr, *Phys. Rev. Lett.* **1982**, *49*, 1691.
[15] J. Contreras-García, Y. Weitao, *Acta Phys.-Chim. Sin.* **2018**, *34*, 567.
[16] M. Ernst, A. Genoni, P. Macchi, *J. Mol. Struct.* **2020**, *1209*, 127975.
[17] E. Prince, in *Mathematical Techniques in Crystallography and Materials Science*, Springer, Berlin, Heidelberg, **1994**, Chapter Estimation of Uncertainty, pp. 95–106.
[18] I. Bytheway, D. J. Grimwood, D. Jayatilaka, *Acta Crystallogr. Sect. A* **2002**, *58*, 232–243.
[19] I. Bytheway, D. J. Grimwood, B. N. Figgis, G. S. Chandler, D. Jayatilaka, *Acta Crystallogr. Sect. A* **2002**, *58*, 244–251.
[20] D. J. Grimwood, I. Bytheway, D. Jayatilaka, *J. Comput. Chem.* **2003**, *24*, 470–483.
[21] S. Grabowsky, D. Jayatilaka, S. Mebs, P. Luger, *Chem. Eur. J.* **2010**, *16*, 12818–12821.
[22] A. Genoni, *J. Phys. Chem. Lett.* **2013**, *4*, 1093–1099.
[23] A. Genoni, *J. Chem. Theory Comput.* **2013**, *9*, 3004–3019.
[24] A. Savin, *J. Mol. Struct.* **2005**, *727*, 127–131.
[25] A. Savin, O. Jepsen, J. Flad, O. K. Andersen, H. Preuss, H. G. von Schnering, *Angew. Chem. Int. Ed. Engl.* **1992**, *31*, 187–188.
[26] D. Jayatilaka, D. Grimwood, *Acta Crystallogr. Sect. A* **2004**, *60*, 111–119.
[27] A. Genoni, L. H. Dos Santos, B. Meyer, P. Macchi, *IUCrJ* **2017**, *4*, 136–146.
[28] J. Contreras-García, P. Mori-Sánchez, B. Silvi, J. Recio, *J. Chem. Theory Comput.* **2009**, *5*, 2108–2114.
[29] J. Contreras-García, R. A. Boto, F. Izquierdo-Ruiz, I. Reva, T. Woller, M. Alonso, *Theor. Chem. Acc.* **2016**, *135*, 1–14.
[30] C. Gatti, P. J. MacDougall, R. F. Bader, *J. Chem. Phys.* **1988**, *88*, 3792–3804.
[31] C. Outeiral, M. A. Vincent, Á. M. Pendás, P. L. Popelier, *Chem. Sci.* **2018**, *9*, 5517–5529.
[32] Y.-G. Wang, C. Matta, N. H. Werstiuk, *J. Comput. Chem.* **2003**, *24*, 1720–1729.
[33] A. J. Cohen, P. Mori-Sánchez, W. Yang, *Science* **2008**, *321*, 792–794.
[34] R. Boese, N. Niederprüm, D. Bläser, A. Maulitz, M. Y. Antipin, P. R. Mallinson, *J. Phys. Chem. B* **1997**, *101*, 5794–5799.
[35] D. Jayatilaka, D. J. Grimwood in *International Conference on Computational Science*, **2003**, Chapter Tonto: a fortran based object-oriented system for quantum chemistry and crystallography, pp. 142–151.
[36] A. D. Becke, *J. Chem. Phys.* **1996**, *104*, 1040–1046.
[37] C. Lee, W. Yang, R. G. Parr, *Phys. Rev. B* **1988**, *37*, 785.
[38] F. Weigend, R. Ahlrichs, *Phys. Chem. Chem. Phys.* **2005**, *7*, 3297–3305.
[39] R. Dovesi, R. Orlando, A. Erba, C. M. Zicovich-Wilson, B. Civalleri, S. Casassa, L. Maschio, M. Ferrabone, M. De L Pierre, P. d'Arco, et al., *Int. J. Quantum Chem.* **2014**, *114*, 1287–1317.
[40] A. Savin, R. Nesper, S. Wengert, T. F. Fässler, *Angew. Chem. Int. Ed. Engl.* **1997**, *36*, 1808–1832.
[41] T. Lu, F. Chen, *J. Comput. Chem.* **2012**, *33*, 580–592.
[42] J. Ahrens, B. Geveci, C. Law, *The visualization handbook* **2005**, *717*.
[43] U. Ayachit, *The paraview guide: a parallel visualization application*, Kitware, Inc., **2015**.
[44] T. A. Keith, AIMAll, (Version 19.10.12), TK Gristmill Software, Overland Park KS, USA, **2019**.

Manuscript received: May 27, 2021
Version of record online: September 13, 2021